S-State Dependent Fourier Transform Infrared Difference Spectra for the Photosystem II Oxygen Evolving Complex†

Warwick Hillier and Gerald T. Babcock

Department of Chemistry, Michigan State University, East Lansing, Michigan 48824

Received October 20, 2000; Revised Manuscript Received December 13, 2000

ABSTRACT: Vibrational spectroscopy provides a means to investigate molecular interactions within the active site of an enzyme. We have applied difference FTIR spectroscopy coupled with a flash turnover protocol of photosystem II (PSII) to study the oxygen evolving complex (OEC). Our data show two overlapping oscillatory patterns as the sample is flashed through the four-step S-state cycle that produces O_2 from two H_2O molecules. The first oscillation pattern of the spectra shows a four-flash period four oscillation and reveals a number of new vibrational modes for each S-state transition, indicative of unique structural changes involved in the formation of each S-state. Importantly, the first and second flash difference spectra are reproduced in the 1800−1200 cm^{-1} spectral region by the fifth and sixth flash difference spectra, respectively. The second oscillation pattern observed is a four-flash, period-two oscillation associated with changes primarily to the amide I and II modes and reports on changes in sign of these modes that alternate 0:0:1:1 during S-state advance. This four-flash, period-two oscillation undergoes sign inversion that alternates during the S_1-to-S_2 and S_3-to-S_0 transitions. Underlying this four-flash period two is a small-scale change in protein secondary structure in the PSII complex that is directly related to S-state advance. These oscillation patterns and their relationships with other PSII phenomena are discussed, and future work can initiate more detailed vibrational FTIR studies for the S-state transitions providing spectral assignments and further structural and mechanistic insight into the photosynthetic water oxidation reaction.

Photosystem II (PSII) is a membrane protein complex crucially important for life because of its capability to catalyze the photosynthetic oxidation of water, releasing O_2 as a byproduct of the reaction. The oxidation reaction is initiated in PSII by the capture of photons by the pigment-containing antenna system that then transfers these photons to the reaction center P680. Thereafter, a series of fast electron-transfer reactions results in charge separation and subsequent stabilization reactions, which move the electron through a series of electron acceptors to plastoquinone. The electron hole on $P680^+$ is also shifted, first to a redox-active tyrosine Y_Z and then into an inorganic core of $Mn_4Ca_1Cl_X$, which together constitute the oxygen evolving complex (OEC) that catalyzes the four-electron oxidation of water to O_2 (*1*−*3*).

The concept that emerged in the field quite early was that the OEC operated with a distinct period-four oscillation pattern in O_2 evolution (*4*). This finding was formalized into the S-state nomenclature, which described the partial reactions of the OEC as traversing five intermediate states following single turnover flashes (*5*). Each forward transition is driven by a light flash, and when the S_4 state is attained (which may be S_3 $Y_Z^{\bullet}$), O_2 is released and the S_0 state is regenerated; i.e.,

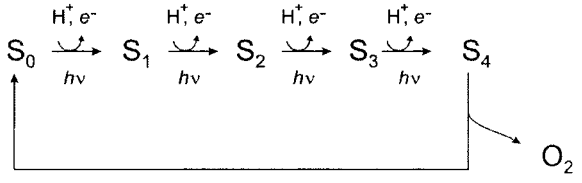

Each S-state transition also has a possibility to undergo a miss (α) or a double hit (β), which effectively desynchronizes the O_2 oscillation pattern after ∼12 flashes (*6*).

Following development of the S-state cycle, research has focused on understanding both the S-state cycle and the structure of the OEC. Recently, the first high-resolution (∼3.7 Å) three-dimensional crystallographic structural information has provided some degree of molecular insight into the OEC (*7*). The reaction mechanism and the formation of the O−O bond by the OEC has been explored by a number of other techniques. For example, various methods have followed rates of electron transfer (*8*, *9*), rates and stoichiometries of proton release (*10*, *11*), oscillations and relaxation phenomena of EPR[1] signals (*12*−*15*), shifts in edge energies derived from XAS measurements (*16*−*18*), and changes in substrate water exchange rates (*19*). Difference Fourier transform infrared (FTIR) spectroscopy in the 1800−1200 cm^{-1} mid-IR regions has also been used to understand the structure of the OEC. This approach has yielded much structural information about the interactions within PSII and the OEC (*20*−*24*). In terms of the S-states, however, the technique has been limited to the S_2/S_1 difference spectrum obtained from the light-induced S_1-to-S_2 transition (*20*−*22*, *24*−*27*). To advance to other S-states, further experimental developments are needed.

To achieve this, we have developed methods to synchronize the S-state advance under conditions suitable for FTIR. To maximize the oscillation pattern, we used nanosecond laser flashes to minimize the double hit (β) parameter, which

† This paper is dedicated to the memory of Jerry Babcock.

[1] Abbreviations: EPR, electron paramagnetic resonance; XAS, X-ray absorption spectroscopy; FTIR, Fourier transform infrared (spectroscopy); MES, 4-morpholinoethanesulfonic acid.

10.1021/bi002436x CCC: $20.00
Published on Web 01/16/2001

is related to flash duration (*6*, *28*). The miss parameter (α), which shows a temperature dependence (*29*), was also reduced by performing our measurements at the lowest possible temperature, here 265 K, which permits S-state advance (*30*) and ensures complete S-state turnover during flash advance. We also sought to avoid artificial quinone acceptors that interact with the Q_A binding sites because of their large contribution in the IR region (*24*) and have used the ferri-/ferrocyanide redox buffer that was developed by Noguchi and Inoue for isolation of PSII donor side contributions (*31*). In this work, we present period-four FTIR oscillations and provide difference spectra for the S_2-to-S_3, the S_3-to-S_0, and the S_0-to-S_1 transitions. These difference spectra provide the first mid-IR FTIR spectroscopic insights into the dynamic structural changes associated with the OEC during each S-state advance. Also observed underlying the period-four S-state cycle is a four-flash, period-two oscillation involving changes of the secondary structure of the OEC. This oscillation behavior is manifested primarily in the amide I and II regions and shows similar spectral features with the S_1-to-S_2 and the following S_2-to-S_3 transition but then reverses on the S_3-to-S_0 transition and persists during the S_0-to-S_1 transition before reversing again. This four-flash, period-two oscillation suggests small-scale conformational changes that are initiated during the S_1-to-S_2 transition and propagate with the next transition before reversing during the S_3-to-S_0 transition. This behavior of the amide I and II likely reflects the movement and rearrangement of a small number of H-bonding partners within PSII during S-state advancement.

MATERIALS AND METHODS

Fresh market spinach was used in the preparation of oxygen evolving PSII membrane fragments according to the standard protocol (*32*) and stored frozen at −80 °C until use. Samples for FTIR measurements were first diluted in 5 mM MES, pH 6.5, 150 mM sucrose, and 5 mM NaCl and centrifuged to a pellet. The PSII electron acceptor 2 mM ferricyanide was added in combination with 18 mM ferrocyanide to generate a redox buffer suitable to remove acceptor-side contributions from the difference spectra (*31*). From the pellet (∼15 mg of Chl/mL), a small quantity of the PSII sample (∼100 μg of Chl) was applied to a BaF window with a spatula in the dark and adjusted such that the amide I region (∼1652 cm^{-1}) was OD ≤ 1.0. The sample was then preflashed with a single 5 mJ/cm^2 flash from a 532 nm Nd:YAG (DCR-1, Quantra-ray) to enrich the population of S_1, dark-adapted for 7 min, loaded into the FTIR cryostat, and cooled to 265 K. The process then required about 45 min to reach temperature stabilization.

FTIR spectroscopy was performed with a Bruker Equinox 55 instrument (Bruker, Billerica, MA) with a MCT detector (MB16, Grasby Infrared, Orlando, FL) and a home-built sample holder and cryostat. The IR optics comprised a KBr beam splitter used in conjunction with a Ge filter (OCLI L02547-9, Santa Ross, CA), which reduced spectral bandwidth and removed the coaxial HeNe beam from the interferometer. A Lake Shore 340 temperature controller and Si diode combination (Lake Shore, Westerville, OH) maintained sample temperatures at 265 K with a precision of ±3 mK. Flash excitation was controlled from the Equinox 55 OPUS interface, and the Nd:YAG was modified to deliver only a single Q-switched flash to the sample during a 10 Hz flashlamp repetition, thus ensuring stability of the laser light intensity. A background spectrum of 100 scans was acquired, and the sample was given a single actinic flash, following which the FTIR was measured for 100 scans. The sample was then given a second actinic flash and was scanned again by FTIR. This protocol was repeated to generate up to eight S-state transitions before the sample was discarded and initiated again with a new sample. Each 100-scan acquisition lasted a duration of ∼25 s, and all spectra were collected at 4 cm^{-1} resolution.

RESULTS

The PSII sample was loaded in the dark following the preflash regime and, after temperature equilibration was reached, was subjected to a series of flashes. Figure 1 shows spectra in the 2200−1800 cm^{-1} region of a sample during a series of flashes. Clearly seen are a trough and a peak at 2115 and 2038 cm^{-1}, respectively, which arise from the changing concentration of the ferri-/ferrocyanide redox buffer. This redox buffer combination was added to oxidize the Q_A^- site (*31*) without oxidizing the non-heme iron center (*33*). The positive peak at 2038 cm^{-1} arises from the increasing concentration of ferrocyanide; conversely, the negative peak at 2115 cm^{-1} arises from the decreasing concentration of ferricyanide as it is reduced by PSII (*34*). The insets of Figure 1 show the amplitudes of the 2038 cm^{-1} peak increasing and the 2115 cm^{-1} peak decreasing as a function of flash. The linear amplitude changes of these peaks with flash number indicate that the same quantitative reduction occurs with each light flash, and the difference in the relative absorption is resulting from the differing extinction coefficients of the two molecules.

To determine that the laser flashes were saturating, we used a 20% neutral density filter to attenuate the flash. This was done after flash 5 in separate series of measurements. At the intensities used for the period-four experiments, we observed behavior identical to that in the inset to Figure 1: a constant slope showing a uniform increase in ferrocyanide at 2036 cm^{-1} and a uniform depletion of ferricyanide at 2115 cm^{-1}. As we lowered the laser intensity to produce nonsaturation conditions, we observed an immediate decrease in ferrocyanide generation after attenuation. As this behavior was not seen in the experiments reported below, we conclude that the laser pulses were above light saturation.

To record each flash advance of the initially synchronized S-state cycle as a separate difference FTIR spectrum, the spectrum recorded on the immediately preceding flash was subtracted from the current flash spectrum. These difference spectra are presented in Figure 2 as a function of light flash. The background dark − dark difference spectrum is also produced at the bottom and shows that we have a peak-to-peak noise level of 5×10^{-6}. A number of FTIR bands can be seen to oscillate in sign as a function of laser flash. Modes that change lie within the regions assigned to protonated carboxylic acid ν(CO) carbonyl-stretching (1750−1700 cm^{-1}), amide 1 (1700−1620 cm^{-1}), amide II (1565−1515 cm^{-1}), asymmetric $\nu_{asym}(COO^-)$ carboxylate-stretching (1650−1550 cm^{-1}), and symmetric $\nu_{sym}(COO^-)$ carboxylate-stretching (1450−1300 cm^{-1}) modes. These changes are easily visualized in Figure 2 with the vertical tie lines from selected

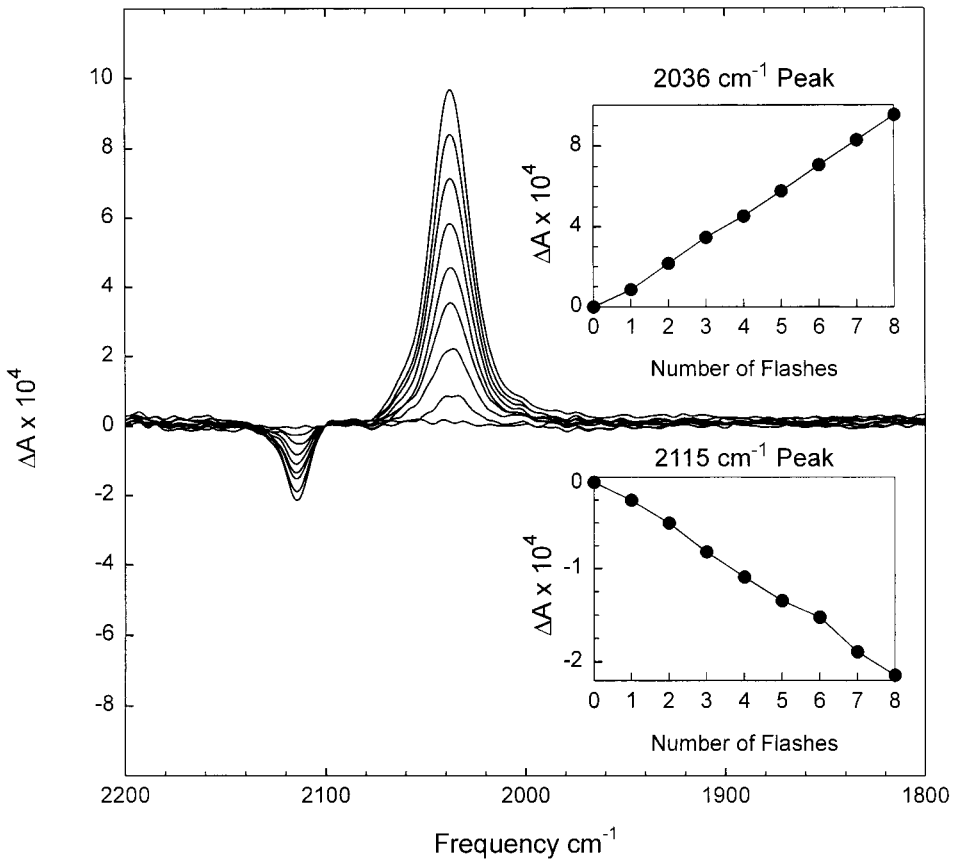

FIGURE 1: FTIR spectra following the flash train for S-state advance showing the changing PSII acceptor concentration of ferricyanide/ferrocyanide as measured from the ferri-/ferrocyanide ν(CN) stretches. Each spectrum was recorded from 100 scans; the spectral resolution was 4 cm^{-1}.

peaks in the S_2/S_1 difference spectra. The difference spectra also appear smaller with each successive flash due to a mixing of the S-state populations. However, the spectral features for the flash 1 FTIR difference spectra in the 1800−1200 cm^{-1} spectral region appear similar to that observed in flash 5. The flash 2 difference spectra also exhibit good resemblance to the flash 6 difference spectra. Furthermore, there is nothing that obviously correlates with the 1:0:1:0 period-two oscillation expected from the acceptor side 1480 cm^{-1} Q_B^- mode (*22*). This latter result indicates the efficiency of the ferri-/ferrocyanide acceptor system. The second oscillation pattern, 0:0:1:1:0:0 for the first six flashes, is shown in Figure 2 to oscillate about the amide 1 and the amide II regions. This pattern shows peaks of approximately similar position (±2 cm^{-1}), which undergo alternation of sign following flashes 3 and 5. This is indicative of a reversible structural change to the protein backbone of the OEC as a function of flash.

Closer examination of the S-state dependence of the mid-IR difference spectra is shown in Figure 3. The flash 1 − dark spectrum generates predominantly the S_2/S_1 difference spectrum, which is seen to be very similar to that reported by various groups (*20*−*22*, *24*, *27*) with characteristic peaks from the ν(CO) stretching from carbonyl side chains [(+)-1747/(−)1737, (+)1718/(−)1708 cm^{-1}] and the backbone ν(CO) stretching amide I region [(−)1677/(+)1668, (−)-1662/(+)1649 cm^{-1}]. The amide I assignments proposed are turns at ∼1673 cm^{-1} giving rise to the (−)1677/(+)1668 cm^{-1} peaks, turns or random coil structure at ∼1665 cm^{-1} to produce the (+)1668/(−)1662 cm^{-1} peaks, α-helical/random coil structures at ∼1655 cm^{-1} giving the (−)1662/(+)1649 cm^{-1} peaks, and β-strands at ∼1642 cm^{-1} that generate modes at (+)1649/(−)1636 cm^{-1}. Also seen are asymmetric $\nu_{asym}(COO^-)$ carboxylate-stretching modes [(−)-1563/(+)1586 cm^{-1}] and symmetric $\nu_{sym}(COO^-)$ carboxylate-stretching modes [(+)1366/(−)1403 cm^{-1}] (*20*, *21*). The protonated carboxylic acid ν(CO) carbonyl stretches in the 1750−1700 cm^{-1} region of Figure 3 [(+)1747/(−)1737, (+)-1718/(−)1708 cm^{-1}] are characteristic for Asp and Glu residues (*35*). The ∼10 cm^{-1} shifts seen on the S_1-S_2 transition are indicative of changes in H-bonding to the carbonyls but do not support the net protonation/deprotonation of these groups during the S_1-S_2 transition (*36*).

The second flash data shown in Figure 3 produce predominantly the S_3/S_2 difference spectrum. The spectrum in Figure 3 shows general similarity to the flash 1 S_2/S_1 difference spectrum in the amide I and II regions. The main difference within the amide I region is an 11 cm^{-1} shift in the S_2/S_1 (−)1677 peak position to (−)1688 cm^{-1}. This change is spectrally suggestive of a modification in the turn/random coil structure of the OEC. Otherwise, the relative positions of the components of the amide I region are of the same sign and within ±2 cm^{-1} of the peaks in the S_2/S_1 difference spectrum. The amide II region shows a strong (−)-1544 cm^{-1} mode, which is also present in the S_2/S_1 difference spectra. This mode originates from the coupled N−H bending (60%) and C−N stretching (40%) modes of the backbone amide II region and demonstrates sensitivity to ^{15}N and ^2H labeling in the S_2/S_1 difference spectrum (*20*, *21*). The S_3/S_2 difference reported here is similar to a preliminary spectrum

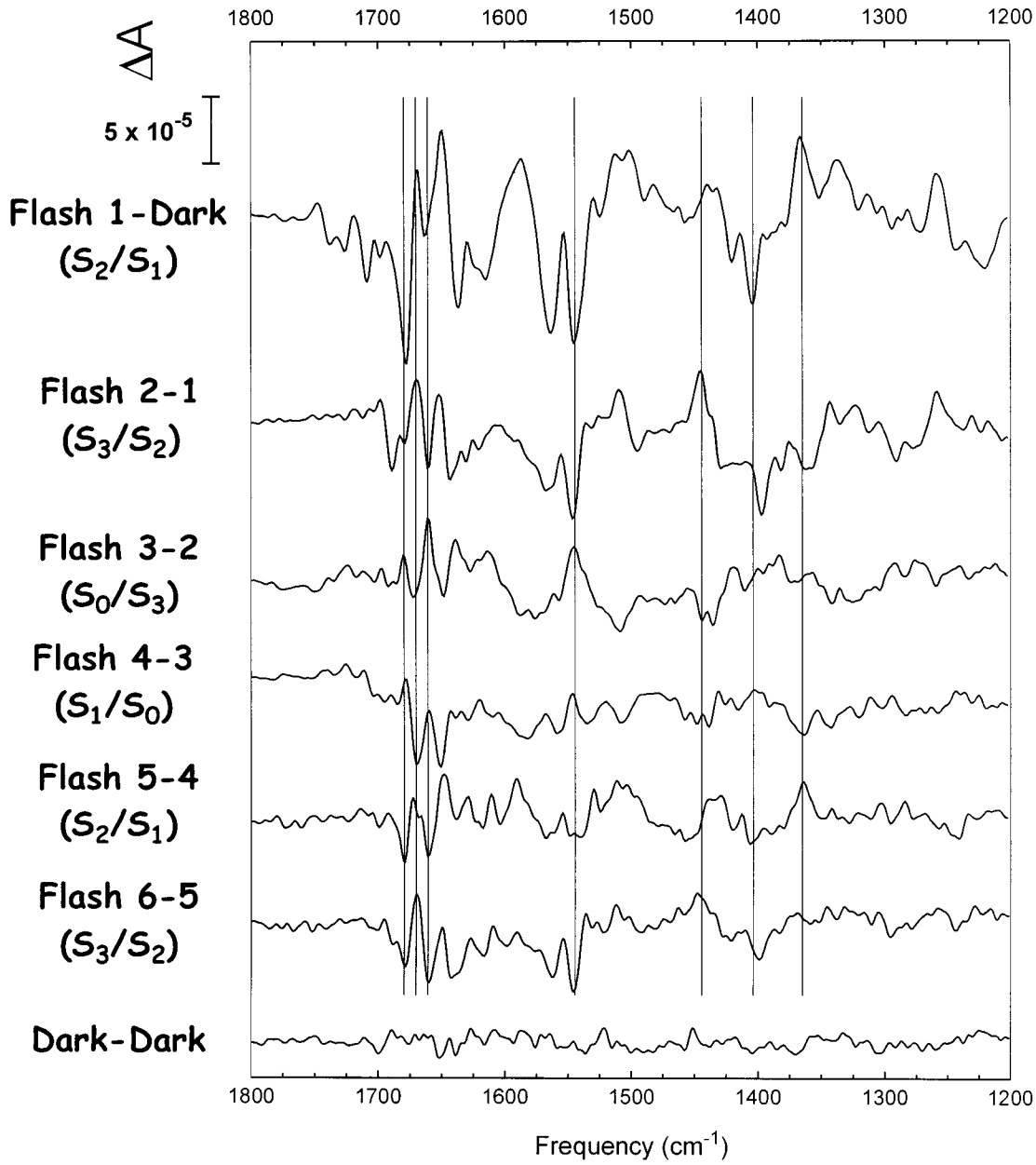

FIGURE 2: FTIR flash-induced difference spectra of PSII membrane fragments at 265 K from the first six flashes given to a dark-adapted S_1-enriched PSII sample. Each S-state advance (7 ns, 532 nm laser flash) was followed by 100 scans of data acquisition (lasting ~25 s), and a total of 20 samples were used to accumulate 2000 spectral averages. Following a laser flash, the previous spectrum was subtracted from the current flash spectrum to obtain a flash − background difference spectrum. All spectra were recorded at 4 cm^{-1} resolution.

reported in core samples containing a greater S_1 contamination (*37*).

In the S_3/S_2 difference spectrum, the changes outside of the amide I and II regions provide a spectral signature for the S_2-S_3 transition. The region containing the symmetric carboxylate-stretching modes (1450−1300 cm^{-1}) undergoes significant changes and shows new modes at (+)1444/(−)-1396 cm^{-1} and at (−)1361/(+)1342 cm^{-1}. These modes reveal what is likely to be new information concerning carboxylate ligands to the OEC. Thus, in addition to the (−)-1403/(+)1366 cm^{-1} pair from the S_1-to-S_2 transition (*20*, *21*), the new bands arising during the S_2-to-S_3 transition strongly implicate the involvement of at least a second carboxylate ligand, which undergoes a change during this transition. The flash 2 − 1 difference spectrum reveals a strong pair of modes at (+)1509/(−)1494 cm^{-1}, which suggests a 15 cm^{-1} upshift of a band upon the S_2-to-S_3 transition. The S_3/S_2 difference spectrum also shows no apparent activity from the carbonyl ν(CO) stretches in the 1750−1700 cm^{-1} region. This contrasts the S_2/S_1 difference spectrum, which shows at least two modes that respond to what is likely to be a change in H-bonding status.

The flash 3 − 2 spectrum generates predominantly the S_0/S_3 difference spectrum, and this shows many significant changes compared to the preceding difference spectra. Clearly seen are changes in the amide I and II regions of the spectrum, which undergo inversion of sign compared to the S_2/S_1 and S_3/S_2 difference spectra. This indicates changes to the secondary structure of the OEC upon the S_3-to-S_0 transition. This step corresponds to the release of the O_2 product and presumed reloading of both substrate water molecules (*2*, *15*, *19*). There are also a number of weak ν-

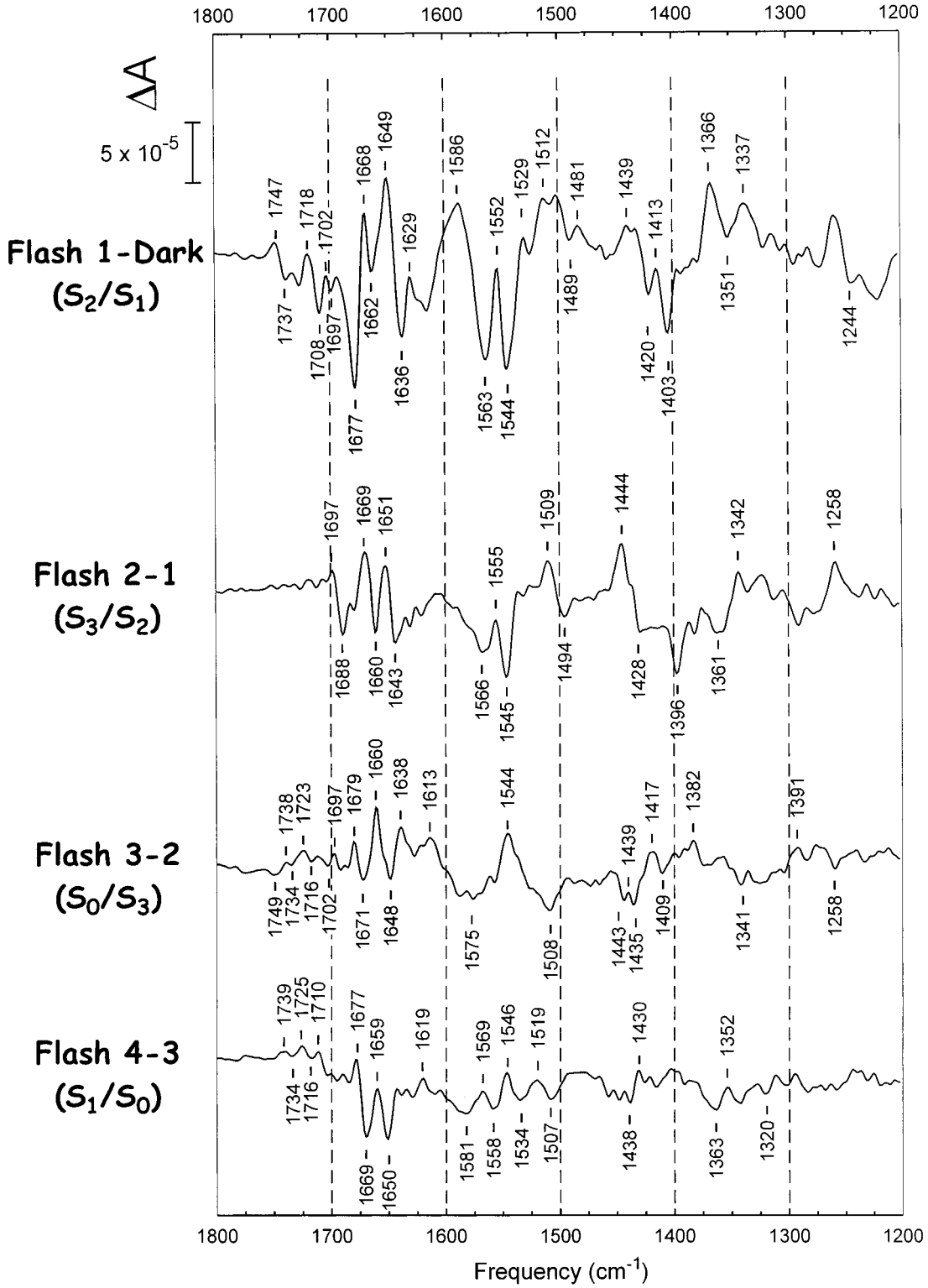

FIGURE 3: Detailed FTIR difference spectra for PSII membrane fragments at 265 K from the first four flashes given to a dark-adapted S_1-enriched PSII sample. Each spectrum is the summation of 20 samples (2000 total scans per flash); and, following a laser flash, the previous spectrum was subtracted from the current flash spectrum to obtain a flash − background difference spectrum. All spectra were recorded at 4 cm^{-1} resolution.

(CO) modes in the 1750−1700 cm^{-1} region of Figure 3, some of which appear to mirror the changes in the S_2/S_1 difference spectrum. This result indicates the reversal of the H-bonding changes initiated during the S_1-S_2 transition. Several additional new spectral bands are observed [(−)-1443/(+)1439/(−)1435, (+)1417/(−)1409/(+)1382] in the region ascribed to symmetric $\nu_{sym}(COO^-)$ carboxylate-stretching modes and numerous ν(CH) modes (*36*), which serve to provide a spectral signature for the S_3-to-S_0 transition.

The flash 4 − 3 spectrum in Figure 3 generates predominantly the S_1/S_0 difference spectra, and this shows similarity to the S_0/S_3 spectra in the amide I and II regions. The sign of the associated peaks for the amide I and II regions remains

the same as for the preceding S_3-to-S_0 transition, although small changes on the order of ± 2 cm^{-1} to the peak positions are apparent. In other spectral regions, however, the flash 4 spectrum shows significant spectral distinction compared to the flash 3 difference spectrum. Additional bands are seen at (−)1581/(+)1569, (−)1558/(+)1546, (−)1534/(+)1519, and (−)1507 cm^{-1}, and also some modes, characteristic of symmetric carboxylate stretching, are observed at (−)1438/(+)1430 cm^{-1}.

DISCUSSION

The results from this work, and those in the accompanying paper by Noguchi and Sugiura (*38*), have provided the first period-four, mid-IR FTIR difference spectra for S-state advance. This behavior is apparent when comparisons are made between the spectra generated in flashes 5 and 6 and the spectra generated with flashes 1 and 2 (Figure 2). The most striking feature is the oscillatory behavior of the (−)-1403/(+)1366 cm^{-1} S_2/S_1 modes and the (+)1444/(−)1396 cm^{-1} S_3/S_2 modes, which are reproduced in flashes 1 and 5 and flashes 2 and 6, respectively. There are other bands that give complexity to each S-state and also oscillate but are smaller in intensity. Overall, however, the general spectral features are well reproduced.

We also record a four-flash, period-two oscillation of 0:0:1:1:0:0 during S-state advance on the first six flashes. This oscillation is apparent from the changes in sign of amide I and II bands, which show spectral similarity during the S_1-to-S_2 and S_2-to-S_3 transitions, and reverse in sign during the S_3-to-S_0 and S_0-to-S_1 transitions. This phenomenon indicates a change in secondary structure to the OEC. The appearance of these changes suggests that S-state advance perturbs the protein backbone of PSII; and on the basis of the intensity of the changes, which are small compared to the intensity of the overall amide I band, only a small number of residues are likely to be involved. The four-flash, period-two oscillations in the amide I region therefore represent a structural change that is induced during the S_1-to-S_2 transition and then returned during the S_3-to-S_0 transition. The origin of these changes is likely to be the result of small changes associated with the H-bonding network of the OEC to the peptide backbone. Similar small changes in protein backbone modes have been reported in the bacterial reaction center when Q_A is photochemically reduced and the resulting Q_A^-/Q_A difference FTIR spectrum is recorded (*39*).

The S-state-dependent 0:0:1:1 electrochromic band shifts have generally been interpreted as arising from the accumulation of net charge in the OEC with H^+ movement to a nearby base (*10*, *11*). However, changes in dipole have recently also been argued to account for the observed electrochromic changes (*40*). From our current FTIR work, the changes associated with the carbonyl stretching provide some bearing on these ideas for the S_1-to-S_2 transition. The 1750−1700 cm^{-1} region, which contains the carbonyl-stretching ν(CO) modes for protonated Asp and Glu residues, shows the appearance of at least two modes during the S_1-to-S_2 transition (1747/1737 and 1718/1708 cm^{-1}). The FTIR difference spectra in the carbonyl region is then notably quiet on the S_2-to-S_3 transition where there is widely agreed to be net proton release (*2*, *10*, *41*). Thereafter, the S_2/S_1 carbonyl modes appear to reverse during the S_3-to-S_0 or possibly also during the S_0-to-S_1 transitions. Our data indicate that the S_1-to-S_2 transition involves some delocalized movement but not net accumulation of charge involving Asp or Glu residues, as the spectra resemble a differential band rather than a single symmetrical mode attributable to Asp or Glu protonation. Such symmetrical modes can be seen to accompany protonation of Asp and Glu residues in proton pathways in the photosynthetic bacterial reaction centers (*42*) and bacteriorhodopsin (*43*). This delocalized H^+ movement of charge in the OEC during S_0-to-S_1 then reverses on the S_3-to-S_0 transition or on the S_2-to-S_3 transition. These results give no indication that a net charge is accumulated in the protein matrix upon S_2 formation, at least on carboxylic acid side chains. A caveat with this interpretation, however, is that a number of acid/base groups in the protein may be involved, which may diminish the overall intensity of the mode shifts.

One issue that has been addressed by XAS is changes in the Mn−Mn vectors within the OEC during S-state advance. In particular, the S_2-to-S_3 transition is suggested to be accompanied by the lengthening of a Mn−Mn vector from the $Mn_4Ca_1Cl_X$ cluster (*44*). In addition to XAS, interpretations of kinetic measurements have also led to proposals that structural changes within the OEC occur during this transition and that these may accompany the distance change in the Mn−Mn vectors (see ref *45*). The difference FTIR spectrum reports several specific spectral changes, potentially consistent with this observation with spectral changes to amide and carboxylate regions (Figure 3). These changes, however, are by no means unique for the S_2-to-S_3 transition. The specific S_3/S_2 modes considered [(+)1444/(−)1396] appear within the symmetrical carboxylate-stretching region (1450−1300 cm^{-1}) and may be derived from carboxylate residues to the inorganic $Mn_4Ca_1Cl_X$ core (*20*, *21*). In this case, the shifts seen can be correlated directly with metal ligation (*46*). The changes to the carboxylate region then suggest that the OEC may undergo changes in coordination geometry upon the S_2-to-S_3 transition potentially consistent with a distance change between the Mn−Mn vectors. A further possibility is that a carboxylate residue responds to a Mn oxidation increase. The difference then between these new modes and those observed on the S_1-to-S_2 transition is that the S_2/S_1 spectra are assigned to a carboxylate ligand undergoing a change in ligation involving principally a Ca ion (*20*, *21*), although assignment can be challenged on the basis of Sr substitution experiments (*47*). Future work will be needed to clarify the origin of these modes.

With each flash, a loss of spectral intensity is apparent in the difference spectra (Figure 2). This is brought about by the miss (α) contribution to the Kok cycle, which is accentuated in this work due to the ∼25 s delay between each of the flashes necessary to allow FTIR data acquisition. Direct estimation of the Kok damping parameter from intensity, as is typified in the O_2 oscillation flash patterns, is made difficult in this work because each spectrum is generated as a difference, and changes in sign to the signals and their underlying spectral shifts mask a simple yield change at a given wavelength. However, we have attempted to make an estimation of the miss parameter. The Kok equation requires a miss parameter of ∼20% to account for the decrease in amide I intensity between flashes 1 and 5. A 20% miss probability generates a significant mixing factor, and the flash 6 − 5 (S_3/S_2) difference spectrum could,

accordingly, be expected to contain significant spectral overlap. Examination of the flash 6 spectrum (Figure 2) reveals some contamination from S_1 in the negative-going part of the spectrum, but the contribution is less than might have been expected. This finding is consistent with problems arising from spectral shifts associated with difference spectroscopy and indicates our miss parameter likely overestimated. Future work will address normalization routines for more quantitative comparison.

The FTIR difference spectra contain considerable spectral information, which is valuable in unraveling the reaction mechanism for photosynthetic water oxidation. This work has, for the first time, demonstrated the feasibility of obtaining FTIR difference spectra for each S-state transition of the OEC of PSII. Future work from other groups and ourselves will seek to make spectral assignments for the S-state transitions, develop protocols for the use of PSII core preparations, and explore the lower IR spectral region (<1000 cm^{-1}) to examine metal−ligand modes.

ACKNOWLEDGMENT

We thank Prof. Stenbjörn Styring and Drs. Hsui-An Chu and Neil Law for helpful discussions.

REFERENCES

1. Britt, D. R. (1996) in *Oxygenic Photosynthesis: The Light Reactions* (Ort, D. R., and Yocum, C. F., Eds.) pp 137−164, Kluwer Academic Publishers, Dordrecht, The Netherlands.
2. Tommos, C., and Babcock, G. T. (1998) *Acc. Chem. Res. 31*, 18−25.
3. Hoganson, C. W., and Babcock, G. T. (2000) *Met. Ions Biol. Syst. 37*, 613−656.
4. Joliot, P., Barieri, G., and Chabaud, R. (1969) *Photochem. Photobiol. 10*, 309−329.
5. Kok, B., Forbush, B., and McGloin, M. (1970) *Photochem. Photobiol. 11*, 457−475.
6. Joliot, P., and Kok, B. (1975) in *Bioenergetics of Photosynthesis* (Govindjee, Ed.) pp 387−412, Academic Press, New York.
7. Zouni, A., Jordan, R., Schlodder, E., Fromme, P., and Witt, H. T. (2000) *Biochim. Biophys. Acta 1457*, 103−105.
8. Tommos, C., and Babcock, G. T. (2000) *Biochim. Biophys. Acta 1458*, 199−219.
9. Westphal, K., Tommos, C., Cukier, R. I., and Babcock, G. T. (2000) *Biochemistry 39*, 16220−16229.
10. Haumann, M., and Junge, W. (1996) in *Oxygenic Photosynthesis: The Light Reactions* (Ort, D. R., and Yocum, C. F., Eds.) pp 165−193, Kluwer Academic Publishers, Dordrecht, The Netherlands.
11. Schlodder, E., and Witt, H. T. (1999) *J. Biol. Chem. 274*, 30387−30392.
12. Styring, S., and Rutherford, A. W. (1988) *Biochemistry 27*, 4915−4923.
13. Åhrling, K. A., Peterson, S., and Styring, S. (1997) *Biochemistry 36*, 13148−13152.
14. Messinger, J., Robblee, J. H., Yu, W. O., Sauer, K., Yachandra, V. K., and Klein, M. P. (1997) *J. Am. Chem. Soc. 119*, 11349−11350.
15. Britt, R. D., Peloquin, J. M., and Campbell, K. A. (2000) *Annu. Rev. Biophys. Biomol. Struct. 29*, 463−495.
16. Ono, T., Noguchi, T., Inoue, Y., Kusunoki, M., Matsushita, and Oyanagi, H. (1992) *Science 258*, 1335−1337.
17. Roelofs, T. A., Liang, W., Latimer, M. J., Cinco, R. M., Rompel, A., Andrews, J. C., Sauer, K., Yachandra, V. K., and Klein, M. P. (1996) *Proc. Natl. Acad. Sci. U.S.A. 93*, 3335−3340.
18. Luzzolino, L., Dittmer, J., Dörner, W., Meyer-Klaucke, W., and Dau, H. (1998) *Biochemistry 37*, 17112−17119.
19. Hillier, W., and Wydrzynski, T. (2000) *Biochemistry 39*, 4399−4505.
20. Noguchi, T., Ono, T.-A., and Inoue, Y. (1995) *Biochim. Biophys. Acta 1228*, 189−200.
21. Noguchi, T., Ono, T.-A., and Inoue, Y. (1995) *Biochim. Biophys. Acta 1232*, 59−66.
22. Zhang, H., Fisher, G., and Wydrzynski, T. (1998) *Biochemistry 37*, 5511−5517.
23. Berthomieu, C., Hienerwadel, R., Boussac, A., Breton, J., and Diner, B. A. (1998) *Biochemistry 37*, 10547−10553.
24. Chu, H.-A., Gardner, M. T., O'Brien, J. P., and Babcock, G. T. (1999) *Biochemistry 38*, 4533−4541.
25. Noguchi, T., Ono, T.-A., and Inoue, Y. (1993) *Biochim. Biophys. Acta 1143*, 333−336.
26. Noguchi, T., Ono, T.-A., and Inoue, Y. (1992) *Biochemistry 31*, 5953−5956.
27. Onoda, K., Mino, H., and Noguchi, T. (2000) *Photosynth. Res. 63*, 47−57.
28. Jursinic, P. A., and Dennenberg, R. J. (1990) *Biochim. Biophys. Acta 1020*, 195−206.
29. Messinger, J., Schröder, W. P., and Renger, G. (1993) *Biochemistry 32*, 7658−7668.
30. Styring, S., and Rutherford, A. W. (1988) *Biochim. Biophys. Acta* 933, 378−383.
31. Noguchi, T., and Inoue, Y. (1995) *J. Biochem. 118*, 9−12.
32. Berthold, D. A., Babcock, G. T., and Yocum, C. F. (1981) *FEBS Lett. 13*, 231−233.
33. Petrouleas, V., and Diner, B. A. (1986) *Biochim. Biophys. Acta 849*, 264−275.
34. Jones, L. H. (1963) *Inorg. Chem. 2*, 777−780.
35. Yu, S., Venyaminov, and Kalnin, N. N. (1990) *Biopolymers 30*, 1243−1257.
36. Socrates, G. (1994) *Infrared Characteristic Group Frequencies*, 2nd ed., Wiley, Chichester, U.K.
37. Chu, H.-A., Hillier, W., Law, N. A., Sackett, H., Haymond, S., and Babcock, G. T. (2000) *Biochim. Biophys. Acta 1459*, 528−532.
38. Noguchi, T., and Sugiura, M. (2001) *Biochemistry 40*, 1497−1502.
39. Nabedryk, E., Bagley, K. A., Thibodeau, D. L., Bauscher, M., Mäntele, W., and Breton, J. (1990) *FEBS Lett. 266*, 59−62.
40. Tommos, C., Hoganson, C. W., Di Valentin, M., Lydakis-Simantiris, N., Dorlet, P., Westphal, K., Chu, H.-A., McCracken, J., and Babcock, G. T. (1998) *Curr. Opin. Chem. Biol. 2*, 244−252.
41. Rappaport, F., and Lavergne, J. (1991) *Biochemistry 30*, 10004−10012.
42. Nabedryk, E., Breton, J., Hienerwadel, R., Fogel, C., Mäentele, W., Paddock, M. L., and Okamura, M. Y. (1995) *Biochemistry 34*, 14722−14732.
43. Brown, L. S., Sasaki, J., Kandori, H., Maeda, A., Needleman, R., and Lanyi, K. (1995) *J. Biol. Chem. 270*, 27122−27126.
44. Liang, W., Roelofs, T. A., Cinco, R. M., Rompel, A., Latimer, M. J., Yu, W. O., Sauer, K., Klein, M. P., and Yachandra, V. K. (2000) *J. Am. Chem. Soc. 122*, 3399−3412.
45. Messinger, J. (2000) *Biochim. Biophys. Acta 1459*, 481−488.
46. Deacon, G. B., and Phillips, R. J. (1980) *Coord. Chem. Rev. 33*, 227−250.
47. Chu, H.-A., Hillier, W., Law, N. A., and Babcock, G. T. (2001) *Biochim. Biophys. Acta 1503*, 69−82.

BI002436X